Journal Pre-proof

Tuning the nanoscale rippling of graphene with PEGylated gold nanoparticles and ion irradiation

Zoltán Osváth , Dániel Zámbó , Attila Sulyok , András Pálinkás , András Deák

Please cite this article as: Zoltán Osváth , Dániel Zámbó , Attila Sulyok , András Pálinkás , András Deák , Tuning the nanoscale rippling of graphene with PEGylated gold nanoparticles and ion irradiation, *Carbon Trends* (2021), doi: https://doi.org/10.1016/j.cartre.2021.100080

Highlights

- Gold nanoparticles of 16 nm diameter were synthesised, and their ordered monolayers were achieved by wet-chemical methods.
- Nanoscale rippling of graphene was induced by transferring the graphene onto the gold nanoparticle monolayer.
- Periodic rippling of graphene was achieved using low-fluence Ar^+ ion irradiation.
- The signatures of irradiation-induced point defects were revealed by scanning tunnelling microscopy and Raman spectroscopy.

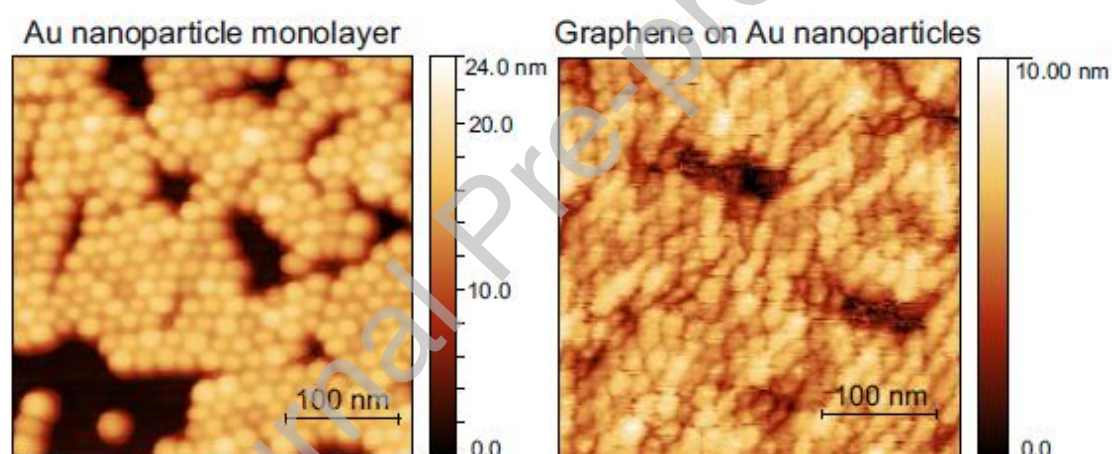# Tuning the nanoscale rippling of graphene with PEGylated gold nanoparticles and ion irradiation

Zoltán Osváth*, Dániel Zámbó, Attila Sulyok, András Pálinkás, and András Deák

Centre for Energy Research, Institute of Technical Physics and Materials Science, 1525 Budapest, P.O. Box 49, Hungary

*Corresponding author: zoltan.osvath@ek-cer.hu

Graphical Abstract

Abstract

Here we report a new method combining strain and defect engineering for the periodic modulation of the graphene nanoscale rippling. First, gold nanoparticles of 16 nm in diameter were synthesized by seed-mediated, wet-chemical approach, and thiol-terminated polyethylene glycol (mPEG-SH) molecules were grafted onto their surface. High-density monolayers of the PEGylated gold nanoparticles were successfully prepared on Si substrates by the Langmuir-Blodgett technique. Graphene grown by chemical vapour deposition was transferred onto the nanoparticle monolayer, and characterized by atomic force microscopy, scanning tunneling microscopy, as well as Raman spectroscopy. The induced nanoscale rippling of graphene was fine-tuned by Ar^+ ion irradiation.

Keywords: graphene ripples, gold nanoparticles, graphene-based hybrid materials, ion irradiation, defect engineering

1. Introduction

Graphene is an intrinsically rippled two-dimensional crystal [1], with the highest known electrical [2] and thermal conductivity [3]. It can be bent and wrinkled as it tolerates very high strain [4,5,6]. Ripples and wrinkles can highly affect the electronic and optical properties of this one-atom thick carbon material; therefore, their controlled realization has been of high interest in the last decade. The spatially varying strain associated with nanoscale ripples can tune the band structure of graphene [7,8], and even open band gaps for specific strain combinations [9]. Corrugations can enhance the chemical activity [10] and functionalization [11,12] of graphene. Calculations show that a local, non-uniform strain [13], or the bi-axial strain associated with graphene ripples lowers the thermal conductivity [14], which can be of significance in increasing the efficiency of graphene-based thermoelectric devices [15,16,17]. Among the many interesting properties of corrugated graphene, it is worth mentioning that – contrary to a flat honeycomb carbon lattice – gas molecules can pass through the ripples, since there the energy barrier of permeation is smaller [18,19].

Structural rippling in graphene can be induced for example by transferring it onto gold nanoparticles (NPs) of high surface coverage prepared by wet-chemical method [20] or by physical methods (thin film evaporation and annealing), as we reported recently [21]. Such graphene/gold nanoparticle hybrid material shows enhanced vapour sensing properties [22]. In this work, we used a different approach to achieve a more ordered rippling of graphene, with better defined rippling period. We applied wet-chemical methods for the preparation of high-density gold nanoparticle monolayers as substrate for graphene, and then polyethylene glycol (mPEG) molecules were attached covalently to gold NPs (PEGylation) *via* the formation of Au-S bonds. This is a commonly used approach for improving drug delivery

[23,24], and to control the interparticle forces between the NPs [25]. The PEG molecules are compatible with organic solvents, which is of crucial importance in the preparation of nanoparticle monolayers on solid substrates. Once the monolayer is formed, it is stable enough for transferring graphene on top of it. Importantly, a regular pattern is formed by NPs at sub-monolayer coverage (see Figure 1), which gives the possibility to fine-tune the structure and properties of graphene in a periodic manner. We present a new method combining strain engineering and ion irradiation for the realization of periodically rippled graphene. The effect of irradiation on the graphene cover layer was revealed by scanning tunneling microscopy (STM), tunneling spectroscopy (STS), and Raman spectroscopy.

2. Experimental

2.1. Gold nanoparticle synthesis and film formation

The nanoparticles have been synthetised according to the protocol published in Ref. [26]. The PEGylation of gold nanoparticles was done with thiol-functionalized methoxy-polyethylene glycol (mPEG-SH) molecules (MW=2000 Da) from *Rapp-Polymere GmbH*, using the procedure described in our earlier work [25]. We aimed to produce the smallest possible nanoparticles and their monolayer, since these are the most interesting for tuning the graphene properties. The Langmuir-Blodgett (LB) films of the nanoparticles have been prepared in a KSV2000 LB-trough. For the film preparation, the PEGylated nanoparticles had been first transferred into ethanol by centrifuging (Eppendorf 5804R) and the alcosol of the nanoparticles was spread at the water/air interface. Prior to transferring the film from the

water/air to the Si substrate/air interface using vertical substrate withdrawal, the compressed monolayer was allowed to relax for 30 min.

2.2. Preparation of graphene-covered gold nanoparticles

Single-layer graphene grown on copper foil substrate was purchased from *Graphenea* Inc. We used a standard screen protector film for the transfer of graphene. An etchant mixture consisting of $CuCl_2$ aqueous solution (20%) and hydrochloric acid (37%) in 4:1 volume ratio was used to etch the copper foil. After the etching procedure, the protector film holding the graphene was rinsed in distilled water, then dried and pressed onto the PEGylated gold nanoparticles. The film was removed, while graphene remained on top of the gold nanoparticles.

In order to fine-tune the nanoscale rippling of graphene, point defects were introduced by Ar^+ ion beam of 1 keV. The irradiation of graphene-coated gold nanoparticle samples was carried out using an ion gun that was built in an ultra-high vacuum surface analytical equipment for ion sputtering purposes. The ion gun (TeleTwin gun made by *Technoorg*, Budapest) was adjusted to 30° angle of incidence and the ion beam was scanned over a 5 mm × 5 mm area. In order to provide low fluence irradiation, the Ar gas supply of the ion gun was extremely reduced (compared to its normal operation) by adjusting the Ar leak valve. Thus, the intensity of the Ar^+ ion beam at the outlet was significantly reduced. The estimated fluence was $\approx 10^{12}$ ions/cm^2, achieved by 20 sec irradiation.

2.3. Characterization

The gold nanoparticle monolayers were imaged using a Zeiss LEO field emission scanning electron microscope (FE-SEM) at an acceleration voltage of 5 keV. Graphene-

6

covered gold nanoparticles were investigated by tapping mode atomic force microscopy (AFM) measurements performed on a Bruker MultiMode 8 apparatus, as well as scanning tunneling microscopy (STM) and tunnelling spectroscopy (STS) measurements using a DI Nanoscope E equipment operating under ambient conditions. The STM measurements were carried out in constant current mode using bias voltages of $1 - 1.2$ V and tunneling currents of $0.3 - 0.5$ nA for large scale imaging. Atomic resolution was achieved with lower bias voltages of $50 - 100$ mV and a current of 1 nA. Inelastic light scattering spectroscopy measurements were performed using a confocal Raman microscope (WITec) and excitation laser of 532 nm. We used laser power of 1 mW, with the beam focused onto $\sim 1\ \mu m^2$ area at the sample surface. The measurements were performed by scanning graphene-covered areas of $20 \times 20\ \mu m^2$, defining 20 scan lines and recording 20 spectra during each scan line. The integration time was 1 sec for each spectrum. The background from gold nanoparticles was removed using the peak analyzer feature of OriginPro software (asymmetric least squares smoothing baseline).

3. Results and discussion

Ordered (sub)monolayer of gold nanoparticles was obtained using the LB method, as shown by SEM and AFM measurements in Fig. 1a and 1b, respectively. Achieving fully ordered state of such small nanoparticles is difficult, nanoparticle voids frequently occur on large-scale. These voids appear as dark-contrasted areas on both SEM and AFM images. In these areas, which show the bare Si substrate, typically $10 - 50$ nanoparticles are missing from the monolayer. Nevertheless, the Si substrate is a good reference point in AFM

7

experiments to measure the height of nanoparticles. We obtained an average nanoparticle height of 16.3 nm (Fig. 1c), and the nanoparticles were closely spaced in ordered clusters with an average interparticle distance of 18 nm. As a comparison, in our previous work [21] where we applied physical preparation methods, we obtained dome-like nanoparticles (typically with height of 15 nm and diameter of 30 nm), while here the nanoparticles are spherical, and the particle size shows a much lower variation.
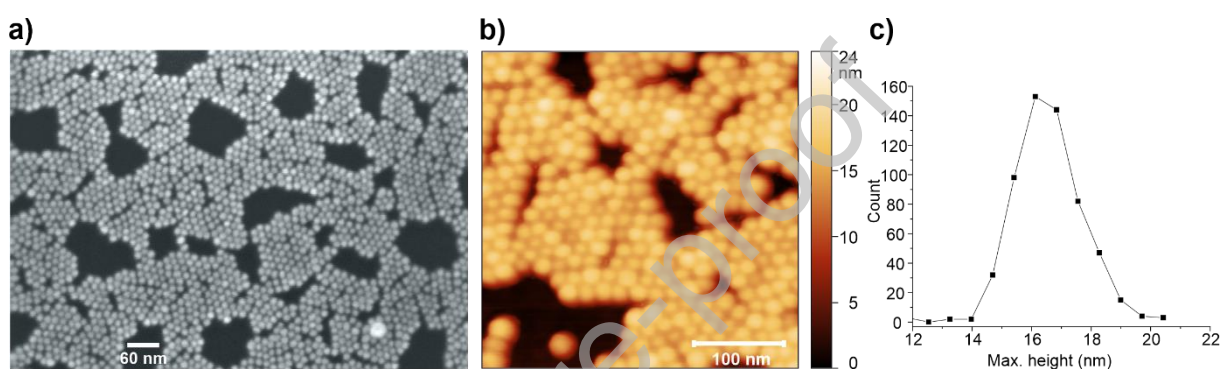
Figure 1. *SEM (**a**) and AFM (**b**) images of the gold nanoparticle monolayer. The height distribution of 589 nanoparticles measured by AFM is shown in **c**). (A colour version of this figure can be viewed online.)*

The structure of graphene transferred onto the PEGylated gold nanoparticle monolayer can be observed in Fig. 2a, which shows the STM image of a completely graphene-covered area. The top of nanoparticles (closely spaced brighter spots), as well as nanoparticle voids (dark-contrasted regions) are both observed.
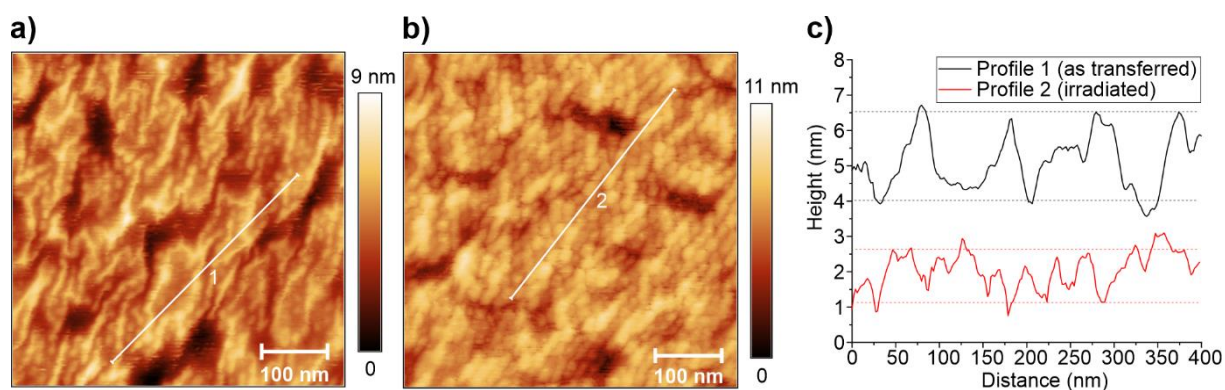
Figure 2. (**a**) STM image of graphene as transferred onto the gold nanoparticle monolayer. (**b**) STM image of graphene supported by nanoparticle monolayer, after ion irradiation. (**c**) The height profiles corresponding to line sections 1 in a) (black line) and 2 in b) (red line). Dashed lines are guide for the eye denoting typical rippling amplitudes. Tunneling parameters: U = 0.5 V, I = 0.5 nA. (A colour version of this figure can be viewed online.)

The graphene is suspended above the voids and has bowl-like shape here. The depth to diameter ratio of these suspended areas is between 5 and 10% (see Fig. S1, Supplementary material). The overall graphene cover has large, elongated ripples, which can be characterized with a typical amplitude of around 2.5 nm, as illustrated in Fig. 2c (height profile no. 1). Our goal here is to minimize these elongated ripples and to impart a rippling periodicity to graphene, which is as close as possible to the periodicity of the underlying nanoparticles. Previously, we achieved this by annealing the graphene-covered gold nanoparticles at 400 °C [21], which improved the adhesion of graphene to the nanoparticles. Here, however, this annealing step is not suitable due to the small size and the wet-chemical preparation method of gold nanoparticles: annealing at several hundreds of degrees Celsius completely impairs the regular assembly of nanoparticles and transforms them into larger, merged particles [27].

9

In order to tune the nanoscale rippling of graphene to match the periodicity of Au NPs, we introduced point defects in the graphene structure by irradiation with 1 keV Ar^+ ions using a fluence of the order 10^{12} ions/cm^2. It was shown recently that both carbon vacancies and Stone-Wales defects induce considerable local out-of-plane deformations in the graphene lattice near the defect [28,29]. We presumed that sufficiently high density of point defects can tune the nanoscale corrugation of the whole graphene sheet. We performed STM investigations of the graphene/mPEG/Au NP hybrid structure after irradiation, and the measurements revealed that indeed, the rippling of graphene changed significantly (Fig. 2b). The elongated ripples disappeared, the typical amplitude of out-of-plane deformations decreased to 1.5 nm (Fig. 2c) and a rippling wavelength of around 30 nm can be observed (Fig. 2c, height profile no. 2). Although this period is larger than the one of the underlying Au NPs, it can be considered as a regular, periodic deformation, characterizing the entire irradiated graphene. Atomic resolution STM measurements revealed hillock-like protrusions, associated with the irradiation-induced point defects, as shown in Figs. 3a and 3b (height profile no. 2).
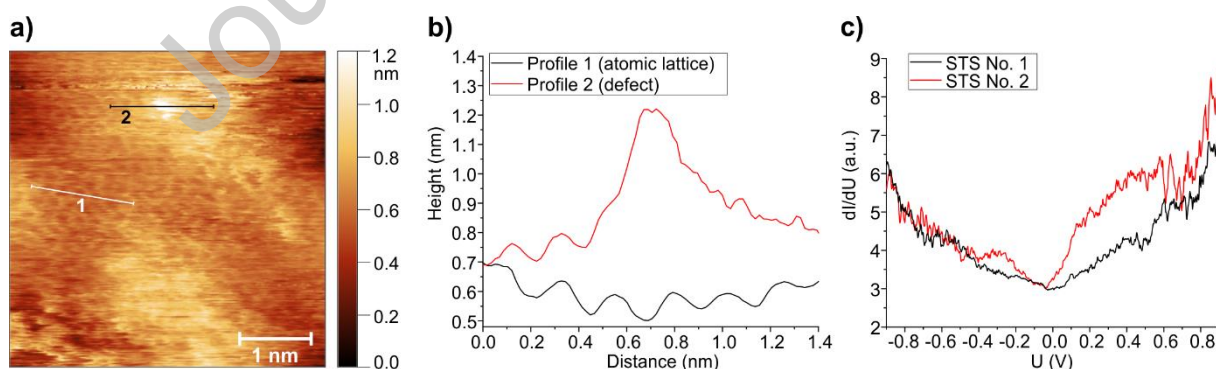

Figure 3. *(a) High resolution STM image of the irradiated graphene shown in Fig. 2b. The height profiles corresponding to unperturbed atomic lattice (section 1) and irradiation-induced point defect (section 2) are shown in (b). (c) STS spectra measured on intact*

graphene area (black) as well as on graphene area with irradiation-induced defect (red). (A colour version of this figure can be viewed online.)

As a comparison, the atomic lattice of intact graphene is also resolved (height profile no. 1). Local *dI/dU* spectra obtained from STS measurements show increased density of states at a defect site (Fig. 3c, red line) for positive bias voltages (*U*), which is the main cause of hillock formation: an apparent increase of height during constant current (*I*) STM imaging [30].

Finally, the gold nanoparticle-supported graphene was measured by Raman spectroscopy, as described in section 2.3. The "as-transferred" graphene is characterized with $I_{2D}/I_G = 2.6 \pm 0.05$ (see Fig. 4), where I_{2D} and I_G are the intensities (heights) of the $2D$ and G peaks, respectively.
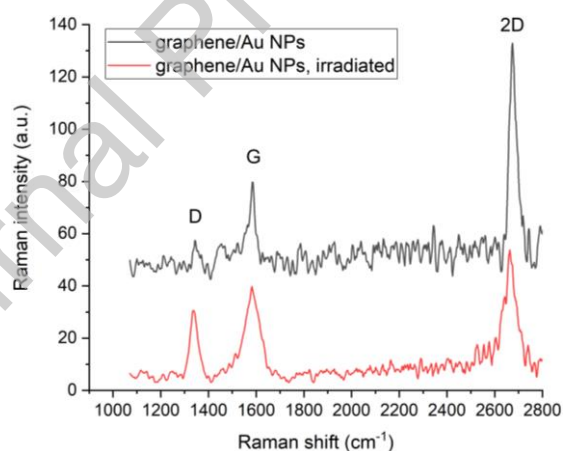
Figure 4. *Average Raman spectra (obtained on $20 \times 20 \ \mu m^2$ areas) of gold nanoparticle-supported graphene "as-transferred" onto the nanoparticles (black), and after ion irradiation (red). For clarity, the background was subtracted, and the spectra were shifted vertically. (A colour version of this figure can be viewed online.)*

It is visible in Fig. 4 that after irradiation the I_{2D}/I_G ratio decreases to 1.25 ± 0.05, while the intensity of the D peak (I_D) increases significantly. In addition, the full width at half maximum of both the G and $2D$ peaks increased from 25.4 to 56.7 cm^{-1} and from 32.3 to 65.2 cm^{-1}, respectively. The broadening of the peaks is a spectroscopic signature of graphene with structural disorder [31], including point defects, clustering of the carbon sp^2 lattice, and bond length disorder [32]. Furthermore, the broadening of the peaks occurs also for increased lattice strain variations at the nanometer-scale [33]. Nanoscale strain variations occur for example due to the nanoparticle voids, where graphene is suspended. The structural deformation of such suspended graphene is different from the periodic rippling of graphene parts that are supported by ordered nanoparticle clusters. The low-fluence ion irradiation induces point defects and local strain variations at the same time, thus the observed broadening of the average peaks is attributed to both effects. Note that after irradiation $I_D/I_G < 1$, as expected for low density of defects [34]. In such case we can estimate the crystalline domain size L_a of irradiated graphene (or average distance between defects) using [35]

$$\frac{I_D}{I_G} = \frac{C(\lambda)}{L_a^2},$$

(1)

where $C(\lambda) = 102 \, nm^2$ for an excitation laser wavelength (λ) of 514 nm [35]. Assuming a similar value for $\lambda = 532 \, nm$ used in the Raman experiments, and using $I_D/I_G = 0.75 \pm 0.05$ extracted from Fig. 4, we obtain $L_a \cong 12 \, nm$, which is in good agreement with the STM observations.

The rippling induced by ion irradiation conveys potentially interesting sensing properties to graphene, since not only the strain at nanoscale, but also the induced point defects can enhance the sensitivity or selectivity upon exposure to gas molecules. Future related work may reveal new properties of such strain- and defect-engineered graphene.

Furthermore, as shown recently, the elastic constant of graphene can be increased by introducing low density of point defects [36]. Thus, combining ion irradiation with the control of nanoscale corrugation can open new paths also to tailor the stiffness of future graphene-based devices.

4. Conclusions

We have prepared monolayers of PEGylated gold nanoparticles with a period of 18 nm. Graphene was successfully transferred onto the NPs. We were able to tune the nanoscale rippling of graphene at the cost of introducing point defects by low fluence ion irradiation. The signatures of irradiation-induced defects were observed by scanning tunneling microscopy and spectroscopy. The crystalline structure of graphene is preserved in domain sizes of the order of 10 nm, as inferred from Raman spectroscopy measurements. Such defective and corrugated graphene coating can be of interest in tailoring the band structure and the functionalization of graphene, as well as in the preparation of enhanced substrates for molecular detection with plasmonic nanoparticles.

CRediT authorship contribution statement

Zoltán Osváth: Conceptualization, Methodology, Formal Analysis and Investigation, Visualization, Writing – Original Draft Preparation, Funding Acquisition. **Dániel Zámbó:** Methodology, Writing – Review & Editing. **Attila Sulyok:** Methodology, Writing – Review & Editing. **András Pálinkás:** Methodology, Formal Analysis and Investigation. **András Deák:** Methodology, Visualization, Writing – Review & Editing, Funding Acquisition.

Declaration of competing interest

The authors declare that they have no known competing financial interests or personal relationships that could have appeared to influence the work reported in this paper.

Acknowledgements

References

1. Fasolino, A.; Los, J.H.; Katsnelson, M.I. Intrinsic ripples in graphene. *Nat. Mater.* **2007**, *6*, 858-861, doi:10.1038/nmat2011.

2. Chen, F.; Xia, J.; Ferry, D. K.; Tao, N. Dielectric Screening Enhanced Performance in Graphene FET. *Nano Lett.* **2009**, *9*, 2571–2574, doi:10.1021/nl900725u.

3. Balandin, A.A.; Ghosh, S.; Bao, W.; Calizo, I.; Teweldebrhan, D.; Miao, F.; Lau, C.N. Superior Thermal Conductivity of Single-Layer Graphene. *Nano Lett.* **2008**, *8*, 902-907, doi:10.1021/nl0731872.

4. Lee, C.; Wei, X.; Kysar, J.W.; Hone, J. Measurement of the Elastic Properties and Intrinsic Strength of Monolayer Graphene. *Science* **2008**, *321*, 385-388, doi:10.1126/science.1157996.

5. Cadelano, E.; Palla, P. L.; Giordano, S.; Colombo, L. Nonlinear Elasticity of Monolayer Graphene. *Phys. Rev. Lett.* **2009**, *102*, 235502, doi:10.1103/PhysRevLett.102.235502.

6. Cao, K.; Feng, S.; Han, Y.; Gao, L.; Hue Ly, T.; Xu, Z.; Lu, Y. Elastic straining of free-standing monolayer graphene. *Nat. Commun.* **2020**, *11*, 284, doi:10.1038/s41467-019-14130-0.

7. Naumis, G.G.; Barraza-Lopez, S.; Oliva-Leyva, M.; Terrones, H. Electronic and optical properties of strained graphene and other strained 2D materials: a review. *Rep. Prog. Phys.* **2017**, *80*, 096501, doi:10.1088/1361-6633/aa74ef.

8. Peng, Z.; Chen, X.; Fan, Y.; Srolovitz, D.J.; Lei, D. Strain engineering of 2D semiconductors and graphene: from strain fields to band-structure tuning and photonic applications. *Light: Sci. Appl.* **2020**, *9*, 190, doi:10.1038/s41377-020-00421-5.

9. Monteverde, U.; Pal, J.; Migliorato, M. A.; Missous, M.; Bangert, U.; Zan, R.; Kashtiban, R.; Powell, D. Under pressure: Control of strain, phonons and bandgap opening in rippled graphene. *Carbon* **2015**, *91*, 266–274, doi:10.1016/j.carbon.2015.04.044.

10. Boukhvalov, D. W.; Katsnelson, M. I. Enhancement of Chemical Activity in Corrugated Graphene. *J. Phys. Chem. C* **2009**, *113*, 14176–14178, doi:10.1021/jp905702e.

11. Drogowska-Horná, K.; Valeš, V.; Plšek, J.; Michlová, M.; Vejpravová, J.; Kalbáč, M. Large scale chemical functionalization of locally curved graphene with nanometer resolution. *Carbon* **2020**, *164*, 207–214, doi:10.1016/j.carbon.2020.04.006.

12. Deng, S.; Rhee, D.; Lee, W.-K.; Che, S.; Keisham, B.; Berry, V.; Odom, T. W. Graphene Wrinkles Enable Spatially Defined Chemistry. *Nano Letters* **2019**, *19*, 5640–5646, doi:10.1021/acs.nanolett.9b02178.

13. Xu, L.; Zhang, X.; Zheng, Y. Local strain effect on the thermal transport of graphene nanoribbons: a molecular dynamics investigation. *Phys. Chem. Chem. Phys.* **2015**, *17*, 12031–12040, doi:10.1039/c4cp06014h.

14. Park, K. H.; Ravaioli, U. Limited thermal transport in rippled graphene induced by bi-axial strain for thermoelectric applications. *J. Appl. Phys.* **2017**, *122*, 025115, doi:10.1063/1.4993911.

15. Zhang, G.; Zhang, Y.-W. Strain effects on thermoelectric properties of two-dimensional materials. *Mech. Mater.* **2015**, *91*, 382–398, doi:10.1016/j.mechmat.2015.03.009.

16. Mani, A.; Benjamin, C. Strained-graphene-based highly efficient quantum heat engine operating at maximum power. *Physical Review E* **2017**, *96*, 032118, doi:10.1103/PhysRevE.96.032118.

17. Zong, P.-A.; Liang, J.; Zhang, P.; Wan, C.; Wang, Y.; Koumoto, K. Graphene-Based Thermoelectrics. *ACS Appl. Energy Mater.* **2020**, *3*, 2224–2239, doi:10.1021/acsaem.9b02187.

18. Liang, T.; He, G.; Wu, X.; Ren, J.; Guo, H.; Kong, Y.; Iwai, H.; Fujita, D.; Gao, H.; Guo, H.; Liu, Y.; Xu, M. Permeation through graphene ripples. *2D Mater.* **2017**, *4*, 025010, doi:10.1088/2053-1583/aa59ca.

19. He, G.; Liang, T.; Wang, Q.; Xu, M.; Liu, Y. Increased permeability of oxygen atoms through graphene with ripples. *Soft Matter* **2017**, *13*, 3994–4000, doi:10.1039/c7sm00607a.

20. Du, Y.; Zhao, Y.; Qu, Y.; Chen, C.-H.; Chen, C.-M.; Chuang, C.-H.; Zhu, Y. Enhanced light–matter interaction of graphene–gold nanoparticle hybrid films for high-performance SERS detection. *J Mater. Chem. C* **2014**, *2*, 4683–4691, doi:10.1039/c4tc00353e.

21. Osváth, Z.; Deák, A.; Kertész, K.; Molnár, G.; Vértesy, G.; Zámbó, D.; Hwang, C.; Biró, L. P. The structure and properties of graphene on gold nanoparticles. *Nanoscale* **2015**, *7*, 5503–5509, doi:10.1039/c5nr00268k.

22. Piszter, G.; Kertész, K.; Molnár, G.; Pálinkás, A.; Deák, A.; Osváth, Z. Vapour sensing properties of graphene-covered gold nanoparticles. *Nanoscale Adv.* **2019**, *1*, 2408–2415, doi:10.1039/c9na00110g.

23. Suk, J. S.; Xu, Q.; Kim, N.; Hanes, J.; Ensign, L. M. PEGylation as a strategy for improving nanoparticle-based drug and gene delivery. *Adv. Drug Deliv. Rev.* **2016**, *99*, 28–51, doi:10.1016/j.addr.2015.09.012.

24. Reznickova, A.; Slavikova, N.; Kolska, Z.; Kolarova, K.; Belinova, T.; Hubalek Kalbacova, M.; Cieslar, M.; Svorcik, V. PEGylated gold nanoparticles: Stability, cytotoxicity and antibacterial activity. *Colloids Surf. A, Physicochem. Eng. Asp.* **2019**, *560*, 26–34, doi:10.1016/j.colsurfa.2018.09.083.

25. Zámbó, D.; Radnóczi, G. Z.; Deák, A. Preparation of Compact Nanoparticle Clusters from Polyethylene Glycol-Coated Gold Nanoparticles by Fine-Tuning Colloidal Interactions. *Langmuir* **2015**, *31*, 2662–2668, doi:10.1021/la504600j.

26. Ziegler, C.; Eychmüller, A. Seeded Growth Synthesis of Uniform Gold Nanoparticles with Diameters of 15−300 nm. *J. Phys. Chem. C* **2011**, *115*, 4502–4506, doi:10.1021/jp1106982.

27. Bechelany, M.; Maeder, X.; Riesterer, J.; Hankache, J.; Lerose, D.; Christiansen, S.; Michler, J.; Philippe, L. Synthesis Mechanisms of Organized Gold Nanoparticles: Influence of Annealing Temperature and Atmosphere. *Cryst. Growth Des.* **2010**, *10*, 587–596, doi:10.1021/cg900981q.

28. Kotakoski, J.; Eder, F. R.; Meyer, J. C. Atomic structure and energetics of large vacancies in graphene. *Phys. Rev. B* **2014**, *89*, 201406(R), doi:10.1103/PhysRevB.89.201406.

29. Sagar, T. C.; Chinthapenta, V.; Horstemeyer, M. F. Effect of defect guided out-of-plane deformations on the mechanical properties of graphene. *Fuller. Nanotub. Car. N.* **2020**, *29*, 83-99, doi:10.1080/1536383X.2020.1813720.

30. Osváth, Z.; Vértesy, G.; Tapasztó, L.; Wéber, F.; Horváth, Z. E.; Gyulai, J.; Biró, L. P. Atomically resolved STM images of carbon nanotube defects produced by Ar^{+} irradiation. *Phys. Rev. B* **2005**, *72*, 045429, doi:10.1103/PhysRevB.72.045429.

31. Eckmann, A.; Felten, A.; Verzhbitskiy, I.; Davey, R.; Casiraghi, C. Raman study on defective graphene: Effect of the excitation energy, type, and amount of defects. *Phys. Rev. B* **2013**, *88*, 035426, doi:10.1103/physrevb.88.035426.

32. Ferrari, A. C. Raman spectroscopy of graphene and graphite: Disorder, electron–phonon coupling, doping and nonadiabatic effects. *Solid State Commun.* **2007**, *143*, 47–57, doi:10.1016/j.ssc.2007.03.052.

33. Neumann, C.; Reichardt, S.; Venezuela, P.; Drögeler, M.; Banszerus, L.; Schmitz, M.; Watanabe, K.; Taniguchi, T.; Mauri, F.; Beschoten, B.; Rotkin, S. V.; Stampfer, C. Raman spectroscopy as probe of nanometre-scale strain variations in graphene. *Nat. Commun.* **2015**, *6*, 8429, doi:10.1038/ncomms9429.

34. Cançado, L. G.; Jorio, A.; Ferreira, E. H. M.; Stavale, F.; Achete, C. A.; Capaz, R. B.; Moutinho, M. V. O.; Lombardo, A.; Kulmala, T. S.; Ferrari, A. C. Quantifying Defects in Graphene via Raman Spectroscopy at Different Excitation Energies. *Nano Lett.* **2011**, *11*, 3190–3196, doi:10.1021/nl201432g.

35. Lucchese, M. M.; Stavale, F.; Ferreira, E. H. M.; Vilani, C.; Moutinho, M. V. O.; Capaz, R. B.; Achete, C. A.; Jorio, A. Quantifying ion-induced defects and Raman relaxation length in graphene. *Carbon* **2010**, *48*, 1592–1597, doi:10.1016/j.carbon.2009.12.057.

36. López-Polín, G.; Gómez-Navarro, C.; Parente, V.; Guinea, F.; Mikhail; Pérez-Murano, F.; Gómez-Herrero, J. Increasing the elastic modulus of graphene by controlled defect creation. *Nat. Phys.* **2015**, *11*, 26–31, doi:10.1038/nphys3183.